Eur Radiol (2007) 17: 3157–3165
DOI 10.1007/s00330-007-0700-4

Yoon Kyung Kim
Kyung Soo Lee
Man Pyo Chung
Joungho Han
Semin Chong
Myung Jin Chung
Chin A Yi
Ha Young Kim

Pulmonary involvement in Churg-Strauss syndrome: an analysis of CT, clinical, and pathologic findings

Received: 24 November 2006
Revised: 6 April 2007
Accepted: 1 June 2007
Published online: 29 June 2007

Y. K. Kim · K. S. Lee (✉) · S. Chong · M. J. Chung · C. A. Yi · H. Y. Kim
Department of Radiology and Center for Imaging Science, Samsung Medical Center, Sungkyunkwan University School of Medicine,
Seoul, 135-710, South Korea
e-mail: kyungs.lee@samsung.com
Tel.: +82-2-34102518
Fax: +82-2-34102559

M. P. Chung
Division of Pulmonary and Critical Care Medicine, Department of Medicine, Samsung Medical Center, Sungkyunkwan University School of Medicine,
Seoul, 135-710, South Korea

J. Han
Department of Pathology, Samsung Medical Center, Sungkyunkwan University School of Medicine,
Seoul, 135-710, South Korea

Abstract We tried to assess retrospectively thin-section CT findings of Churg-Strauss syndrome (CSS) in 25 patients and to compare these findings with clinical and histopathologic findings. Of 25 patients, 19 (76%) had parenchymal abnormalities at CT; small nodules (n=12; 63%), ground-glass opacity (n=10; 53%), bronchial wall thickening (n=10; 53%), and consolidation (n=8; 42%). Parenchymal abnormalities (n=19) were categorizable as an airway pattern in 11 and an airspace pattern in eight. Patients with an airway pattern (n=5) had obstructive (n=3) or combined (n=2) PFT results, whereas those with an airspace pattern (n=4) had restrictive (n=3) or obstructive (n=1) results. Parenchymal opacities at CT corresponded histologically to areas of eosinophilic pneumonia, necrotizing granulomas, and granulomatous vasculitis; small nodules to eosinophilic bronchiolitis and peribronchiolar vasculitis; and bronchial wall thickening to airway wall eosinophil and lymphocyte infiltration. Patients with airspace pattern responded more readily to treatment than those with airway pattern. CT shows lung parenchymal abnormalities in about three-quarters of CSS patients and these abnormalities can be categorized as airspace or airway patterns. This classification helps predict PFT data, underlying histopathology, and treatment response.

Keywords Churg-strauss syndrome · Eosinophilia · Lung · CT · Diseases

Introduction

Since a form of disseminated necrotizing vasculitis that occurs exclusively in asthma patients was first described by Churg and Strauss in 1951 [1], this syndrome has been referred to as allergic granulomatosis and angiitis or Churg-Strauss syndrome (CSS). CSS is histopathologically characterized by eosinophil tissue infiltration, necrotizing vasculitis, and extravascular granulomas. Currently, however, the diagnosis of CSS does not require this pathologic triad, because diseases with these three histopathologic features occur only in a minority of patients [2].

CSS is a rare disease; its incidence is one to three cases per 100,000 adults per year. The principal causes of morbidity and mortality are myocardial infarction secondary to coronary arteritis. Males are affected slightly more frequently than females and the age at onset varies from 15 to 70 years, with the mean age at diagnosis around 50 years [2–4].

The American College of Rheumatology (ACR) classification of CSS (proposed in 1990) includes six criteria, i.e., asthma, eosinophilia of >10% white blood cell count (by differential counting), migratory or transient pulmonary opacities on chest radiographs, mononeuropathy (including multiplex) or polyneuropathy, paranasal sinus abnormalities, and extravascular eosinophils on biopsy [3]. According to this classification, the presence of four or more of these six criteria allows a diagnosis of CSS to be made with a sensitivity of 85% and a specificity of almost 100% [3]. Clinically, CSS is known to be readily diagnosable using the above criteria, and subsequently to respond dramatically to corticosteroid therapy [4].

Although radiologic findings are nonspecific, the most common radiographic findings reported are transient, patchy, and nonsegmental consolidation or small and large nodular opacities [4], whereas the most common thin-section (TS) CT findings are bilateral subpleural ground-glass opacity (GGO) or consolidation and small centrilobular nodules [5, 6]. However, these reports are based on relatively small numbers of patients. Thus, the purpose of this study was to analyze retrospectively the TSCT findings of 25 CSS patients and to compare these findings with pulmonary functional test (PFT) results, underlying histopathologies, and clinical patient treatment responses as determined by follow-up studies.

Materials and methods

Patients, CT acquisition, and analysis

Between September 1995 and June 2006, we enrolled 25 consecutive patients (male:female=12:13, mean age 45± 13.4 years) who fulfilled the American College of Rheumatology diagnostic criteria for CSS. Eight of these 25 patients were smokers (2–125 pack years, mean 39±42.3 pack years).

CT scans of the thorax were obtained at the time of the initial diagnosis and as part of the diagnostic work up in all 25 patients. All CT scans were obtained using commercially available CT scanners (a single-detector CT scanner: HiSpeed Advantage, GE Medical Systems, Milwaukee, Wis.; a four-detector CT scanner: LightSpeed QXi, GE Medical Systems, Milwaukee, Wis.; an eight-detector CT scanner: LightSpeed Ultra, GE Medical Systems, Milwaukee, Wis.). TSCT scans of the thorax, obtained using 1.0-mm collimation, at 10-mm intervals, without intravenous contrast medium injection, were available in all patients. All CT data were reconstructed using a high-spatial-frequency (bone) algorithm. Scan data were displayed directly on four monitors (using 1,536×2,048 image matrices, 8-bit viewable gray scale, and 60-ft-Lambert luminescence) of a picture archiving and communication system (Pathspeed or Centricity 2.0; GE Medical Systems Integrated Imaging Solutions, Mt Prospect, Ill.). CT scans were displayed at mediastinal (window width, 400 HU; window level, 20 HU) and lung window (window width, 1,500 HU; window level, -700 HU) settings.

Two chest radiologists (with 3 and 16 years of thoracic CT interpretation experience, respectively) reviewed CT images together, and made decisions concerning CT findings by consensus. We assessed the presence and distribution of lung parenchymal abnormalities. We also noticed the presence of pleural effusion and of mediastinal or hilar lymphadenopathy. Nodal stations were classified according to the lymph node map definition for lung cancer staging proposed by Mountain and Dresler [7]. Mediastinal nodes were considered abnormal when they were greater than 10 mm in short-axis diameter and hilar nodes when greater than 10 mm in long-axis diameter. Lung parenchymal abnormalities were analyzed in terms of consolidation, ground-glass opacity (GGO), nodules (10–30 mm in diameter), small nodules (<10 mm in diameter), and reticulation. The presences of interlobular septal thickening, tree-in-bud opacity sign, mosaic perfusion pattern, bronchial wall thickening, bronchial dilatation, and reversed halo sign (central ground-glass opacity and surrounding consolidation) [8] were also recorded. Consolidation was defined as an area of opacification that obscured the underlying vessels; GGO was defined as a hazy increase in lung attenuation with no obscuration of underlying vessels; tree-in-bud sign was defined as nodular dilatation of centrilobular branching structures resembling a budding tree; and mosaic perfusion pattern was defined as a patchwork of regions of varied attenuation secondary to regional differences in perfusion [9, 10]. After recording the lobes with the above patterns of abnormalities, distribution of parenchymal abnormalities on CT scans were categorized as: unilateral or bilateral; peripheral (within 2 cm from the visceral pleura), central (within 3 cm from the hilum or the mediastinum), or random in the transverse plane; upper (superior to the hilum), lower (inferior to the hilum) or random in the longitudinal plane; and as peribronchovascular or random. Small nodules were defined as centrilobular (in the central portion of the secondary pulmonary lobule) or perilobular (in the periphery of the lobule abutting the pleura or the fissure), according to their location within the secondary pulmonary lobule [11].

After analyzing each parenchymal abnormality at TSCT, lung lesions were categorized into airspace or airway pattern. An airspace pattern was defined when parenchymal opacities (consolidation plus GGO) or poorly-defined nodules were the predominant parenchymal abnormalities, whereas an airway pattern was defined when bronchial wall thickening and bronchial dilatation with or without small centrilobular nodule(s), tree-in-bud sign, or mosaic perfusion pattern were the main abnormalities. When the two patterns of parenchymal abnormalities seemed to be relatively similar in extent, thus when lesions could not be allocated to an airspace or airway disease pattern, those were referred to as unclassifiable.

Comparison study between CT findings and functional or histopathologic findings

Of the 19 patients with parenchymal abnormalities at CT, nine underwent pulmonary function test (PFT) using a spirometer (SensorMedics, Yorba Linda, Calif.). CT and PFT were performed within 0–10 days of each other (mean 4±3.3 days, median 2 days). The following PFT parameters were recorded: forced expiratory volume in 1 s (FEV1), forced vital capacity (FVC), and FEV1/FVC ratio. PFT results were expressed as percentages of predicted values of each parameter for each individual based, taking patient age, gender, and height into account [12]. Results were then categorized into three patterns; restrictive (FVC <80% of the predicted value plus an FEV1/FVC of ≥70%), obstructive (FEV1/FVC <70% plus an FVC ≥80% of predicted), or combined pattern. Results were compared with CT patterns (i.e., airspace, airway, and unclassifiable patterns).

We also compared CT findings with histopathologic findings in eight patients with available lung biopsy specimens from a total of ten biopsy sites. The time intervals between CT examination and pathologic diagnosis were 0–11 days (mean, 3 days). Biopsy specimens were obtained by video-assisted thoracoscopic surgery in three patients and by transbronchial lung biopsy in five. Biopsy specimens were obtained from six sites of parenchymal opacity (consolidation plus GGO), two sites of small centrilobular nodules, and one site for nodule and for bronchial wall thickening.

CT-clinical study comparison

Because patients with CSS almost always had asthma, which might have produced bronchial wall thickening with bronchial luminal diameter narrowing or dilatation (an airway pattern) at CT [13] and because CT findings of CSS were classified as patterns of airway or airspace disease, a previous asthma treatment history before CSS diagnosis was correlated with TSCT disease pattern types.

After CSS syndrome was diagnosed, anti-inflammatory drug therapy was administered to 18 patients with pulmonary parenchymal opacities at TSCT except one; prednisone alone was administered in ten and prednisone plus cyclophosphamide in the remaining eight. We also evaluated patient treatment response based on radiographic (n=19, follow-up period 29–3,178 days, mean 1,025±913.9 days) and on CT findings (n=7, follow-up period 69–3,158 days, mean 1,016±1048.1 days) during follow-up. CT patterns (airspace, airway and unclassifiable) were compared in terms of treatment response.

Results

The diagnostic features of the 25 CSS patients are summarized in Table 1.

CT findings

Of the 25 patients, 19 (76%) (male:female=12:7, mean age 43±14.6 years) had pulmonary parenchymal abnormalities at TSCT. The pulmonary abnormalities identified in these 19 patients are summarized in Table 2. CT findings consisted of small nodules (observed in 12 patients: n=12, 63%), GGO (n=10, 53%), bronchial wall thickening (n=10; 53%) or dilatation (n=10; 53%), consolidation (n=8; 42%), interlobular septal thickening (n=8; 42%), and large nodules (n=1, 6%). Tree-in-bud sign (centrilobular small nodules and branching linear structures) was observed in seven (37%) patients and mosaic perfusion pattern in nine (47%).

Parenchymal abnormalities were classified as predominantly an airway pattern in 11 patients and as an airspace pattern in eight.

Small nodules (<10 mm in diameter, identified in 12 patients) (Figs. 1, 2, 3) were centrilobular within the secondary pulmonary lobule in all patients. They were rather random without zonal predominance both on transverse and longitudinal plane images (Table 3). Ground-glass opacity (Fig. 1) observed in ten patients and consolidation (Figs. 1, 2) identified in eight patients, also showed mainly random distribution. Reversed halo sign was observed in one patient (Fig. 1).

Bronchial dilatation and wall thickening had no zonal predominance. Tree-in-bud sign observed in seven patients was predominantly random in distribution. Mosaic perfusion pattern had no zonal predominance. Interlobular septal thickening noticed in eight patients was predominantly peripheral in the transverse plane (Table 3). The septal thickening was present in five (45%) of 11 patients with airway pattern and three (38%) of eight patients with airspace pattern. Eight patients had mediastinal (14 enlarged nodes were observed in 14 nodal stations in these eight patients; station 7 in six patients, 4R in four, 2R in two, 4L and 5 in one each) or hilar lymphadenopathy (three patients had bilateral hilar nodal enlargement). Mediastinal or hilar nodal enlargement was present in three (27%) of 11 patients with airway pattern and five (63%) of eight patients with airspace pattern.

CT-PFT comparisons

In nine patients in whom PFT results were available, functional results were classified as an obstructive pattern in four (one was a smoker), restrictive in three (two were smokers), and combined into two (one was a smokers). In

Table 1 CSS in 25 patients and their fulfilling feature of the American College of Rheumatology (*ACR*) diagnostic criteria (*M* male, *F* female, *PNS* paranasal sinus, *Eo* peripheral blood eosinophil, *NA* not available)

Case No.	Age/Sex	ACR diagnostic criteria of CSS					
		Asthma	PNS Abnormality	Eo >10%	Neuropathy	Transient pulmonary opacities	Extravascular eosinophilia on biopsy
1	32/M	Y	Y	Y (40%)	N	Y	Skin, lung
2	43/M	Y	N	Y (20%)	Y	Y	Skin
3	36/M	Y	N	Y (21%)	Y	Y	Nerve, lung
4	43/F	Y	Y	Y (19%)	N	Y	NA
5	86/M	Y	Y	Y (52%)	Y	Y	Skin, lung
6	52/M	Y	N	Y (51%)	Y	Y	Nerve
7	28/F	Y	N	Y (61%)	N	Y	Lung
8	39/M	Y	N	Y (30%)	N	Y	Lung
9	49/F	Y	Y	Y (31%)	Y	Y	Nerve
10	34/M	Y	Y	Y (49%)	N	Y	NA
11	42/F	Y	Y	Y (23%)	N	Y	Skin
12	25/F	Y	Y	Y (60%)	N	Y	Lung
13	25/M	Y	Y	N (8%)	Y	Y	Nerve
14	29/M	Y	Y	Y (30%)	N	Y	Skin, lung
15	45/M	Y	Y	N (8%)	N	Y	Skin
16	52/M	Y	Y	Y (27%)	Y	Y	Lung
17	60/F	Y	Y	Y (18%)	Y	Y	NA
18	53/M	Y	Y	Y (30%)	N	Y	NA
19	52/F	Y	Y	Y (15%)	Y	Y	Skin
20	56/F	Y	Y	N (3%)	Y	N	Nerve, skin
21	57/F	Y	Y	Y (14%)	Y	N	Nasal cavity
22	37/M	Y	N	Y (26%)	Y	N	Skin
23	49/F	Y	N	Y (56%)	Y	N	Nerve
24	42/F	Y	Y	Y (14%)	Y	N	Nerve
25	53/M	Y	N	Y (70%)	Y	N	Skin

terms of CT pattern-PFT comparisons (n=9) (Table 2), three of five patients with an airway pattern of abnormalities showed obstructive PFT results. Two patients with an airway pattern showed combined PFT results. Three of four patients with an airspace CT pattern had restrictive PFT result patterns. One patient with an airspace pattern showed obstructive PFT results (Table 2).

CT-pathologic comparisons

Consolidation or ground-glass opacities observed at thin-section CT (n=6) corresponded histopathologically to the areas of eosinophilic infiltration in the alveoli and alveolar walls. Some fibrins were mixed with eosinophils in alveolar spaces (Fig. 2). These areas were accompanied by necrotizing granulomas (Fig. 2) and several foci of necrotizing vasculitis involving capillaries were identified in the peribronchial interstitium. Small centrilobular nodules at CT (n=2) corresponded histopathologically to areas of dense eosinophil and lymphocyte infiltration in the bronchiolar walls. Lymphoid follicle formation was also noted in bronchiolar walls. Surrounding scattered areas of necrotizing vasculitis involving capillaries in alveolar walls were also observed (Fig. 3). Nodules (>10 mm in diameter, n=1) at CT represented histologically mixed areas of pulmonary hemorrhage related to vasculitis, necrotizing granulomas, or surrounding eosinophilic infiltration. Bronchial wall thickening (n=1) was caused by eosinophilic and lymphocytic infiltration into airway walls.

CT-clinical comparisons

Of 11 patients with an airway disease pattern, nine (82%) had an asthma treatment history (mean 44±49.6 months, range 6–168 months) (five of the nine were treated with corticosteroids), whereas five (63%) of eight patients with an airspace disease pattern had an asthma treatment history

Table 2 Parenchymal lung abnormalities at thin-section CT and PFT and clinical findings in 19 patients with CSS (*GGO* ground-glass opacity, *NA* not available, *CR* complete remission, *NC* no change, *RU* right upper lobe, *RM* right middle lobe, *RL* right lower lobe, *LU* left upper lobe, *Li* lingular division, *LL* left lower lobe, *PFT* pulmonary function test)

Case no.	CT findings								Initial CT pattern	PFT	Follow-up	Relapse
	Consolidation	GGO	Large nodule	Small Nodule	Tree-in-bud	Mosaic Perfusion	Bronchial wall thickening	Bronchial dilatation				
1	All lobes	All lobes	All lobes	All lobes	RU, RM, RL, Li, LL				Airspace	NA	CR[a]	
2		RU		RL					Airspace	NA	CR	
3	RM, RL, Li, LL	All lobes							Airspace	NA	CR	O
4	All lobes	All lobes		All lobes					Airspace	Obstructive	CR	O
5	RM, RL								Airspace	Restrictive	CR	
6		LU, Li		RL					Airspace	NA	NC	
7	RL, LL	RL, LL		All lobes					Airspace	Restrictive	CR	
8	All lobes	RL, LL		All lobes					Airspace	Restrictive	CR[a]	O
9					RM,RL	All lobes	All lobes	All lobes	Airway	Obstructive	NC[a]	
10						RL	RM, RL		Airway	NA	CR[a]	
11		RU		RU, RL	RU		RU, LU	RU, LU	Airway	NA	NC	O
12		RU, RM, RL, LU, LL		RU, RL, LL	RU, RL, LL	All lobes	All lobes	All lobes	Airway	Combined	CR[a]	O
13				All lobes	RL, LU, LL	RL, Li, LL	All lobes	RU, RM, LU, Li	Airway	Combined	NC	
14				All lobes	All lobes	All lobes	All lobes	All lobes	Airway	Obstructive	CR[a]	O
15						RM, RL, Li, LL	RM, RL, Li, LL	RM, RL, Li, LL	Airway	Obstructive	NC	
16	RL, LL	RM, RL, Li, LL		All lobes		All lobes	RM, RL, Li, LL	RM, RL, Li, LL	Airway	NA	CR[a]	O
17	RU, RM, RL, LU, Li					RL, LU, Li, LL	RL, LU, Li, LL	RL, LU, Li, LL	Airway	NA	NC	
18				RU, RL, LU, LL		RM, RL, LU, LL		RL, LU, LL	Airway	NA	NC	
19					RU, RM, RL, LL		All lobes	LL	Airway	NA	NC	

[a]CR or NC on both chest radiograph and CT

Fig. 1a–c CSS in a 43-year-old woman (patient 4 in Tables 1 and 2). **a** Chest radiograph shows patchy parenchymal opacities (*arrows*) in both lungs. **b**, **c** Transverse lung-window thin-section (1.0-mm thickness) CT scans obtained at levels of main bronchi (**b**) and liver dome (**c**), respectively, demonstrate patchy parenchymal opacities in both lungs (*arrows*) along bronchovascular bundles or in peripheral regions. Some lesions show reversed halo sign (central ground-glass opacity and surrounding consolidation). Also note nodular lesions (*arrowheads*)

(mean 53±43.8 months, range 12–120 months) (three of the five were treated with corticosteroids).

Of 19 patients with parenchymal abnormalities, 11 (58%) experienced complete radiologic remission over a follow-up of 18–140 days (mean 57±41.1 days), but the remaining eight showed no interval changes over a follow-up of 29–3,178 days (mean 930±1,082.2 days) on chest radiographs. Four (within 18–69 days of follow-up, mean

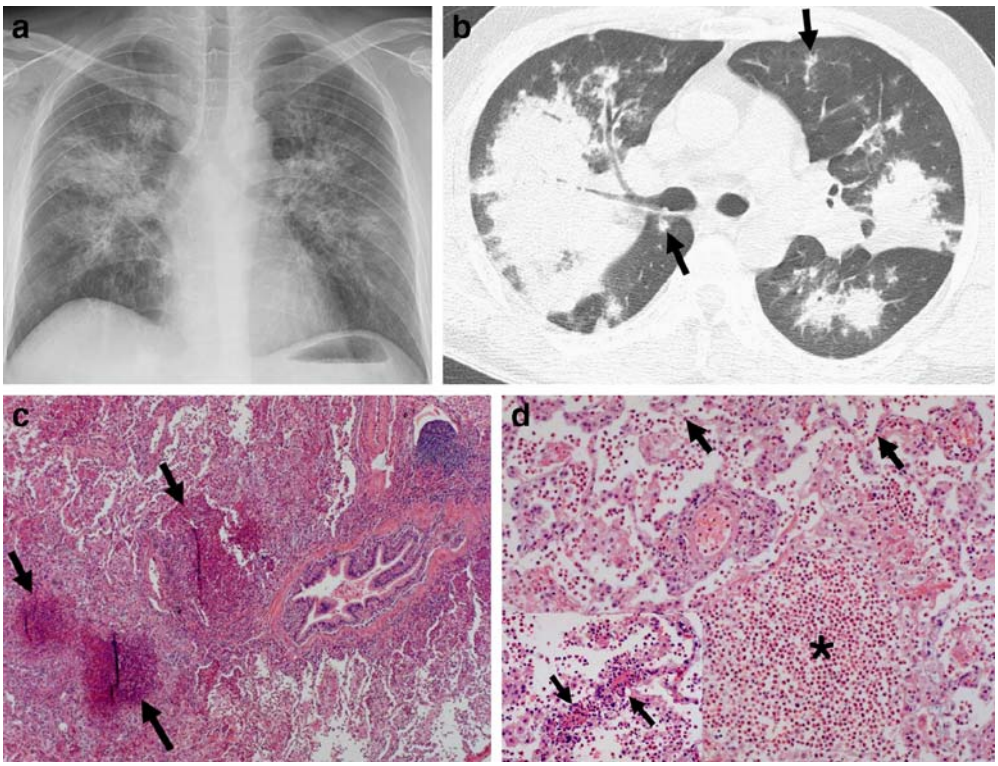

Fig. 2a–d CSS in a 39-year-old man (patient 8 in Tables 1 and 2). **a** Chest radiograph shows patchy parenchymal opacities in both lungs with sparing apices and costophrenic angles. Subcutaneous emphysema in right chest wall was due to pneumothorax (caused by transbronchial lung biopsy) drainage. **b** Transverse lung-window CT (1.0-mm thickness) scan obtained at level of right upper lobar bronchus shows dense parenchymal consolidation in both lungs with random distribution. Also note poorly-marginated small nodules (*arrows*). **c** Medium-magnification photomicrograph shows necrotizing granulomas (*arrows*) containing numerous eosinophils at peribronchiolar interstitium. Adjacent alveolar spaces are also filled with fibrin and eosinophils. (Hematoxylin-eosin stain, original magnification ×40) **d** High-magnification photomicrograph demonstrates area of eosinophilic pneumonia showing numerous eosinophils admixed with fibrin in alveolar spaces (*asterisk*). Also note some eosinophils (*arrows*) in alveolar walls. Nine-month follow-up radiograph with corticosteroid treatment (not shown here) demonstrated completely disappeared parenchymal opacities. *Inset:* focus of vasculitis (*arrows*). (Hematoxylin-eosin stain, original magnification ×100)

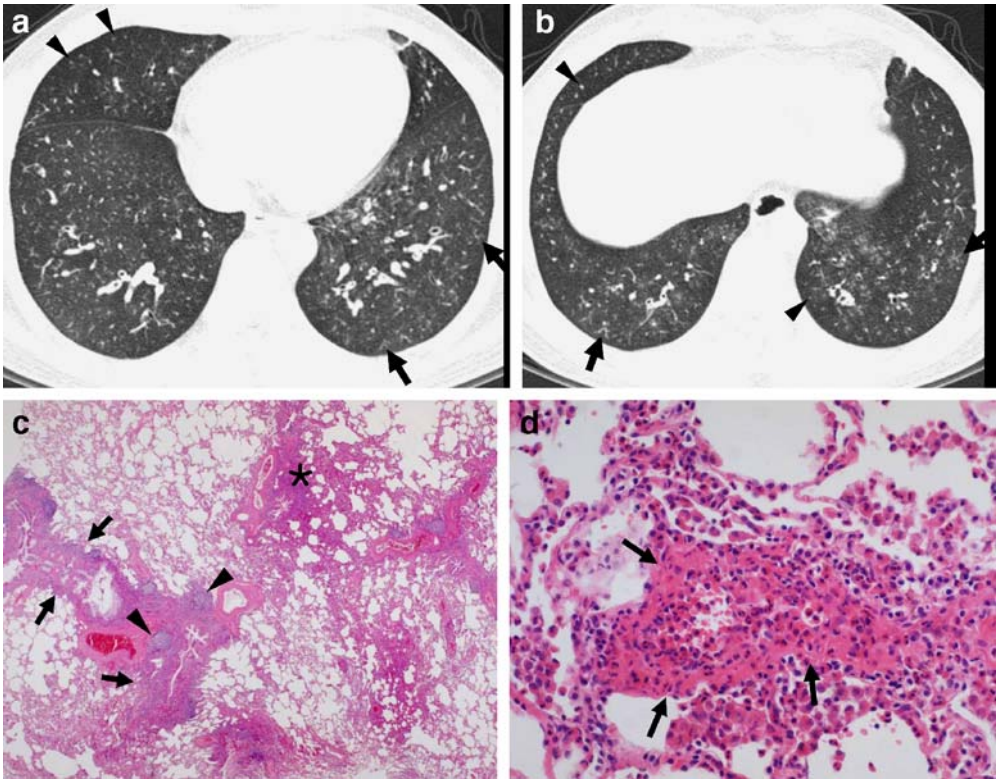

Fig. 3a–d CSS in a 29-year-old man (patient 14 in Tables 1 and 2). **a**, **b** Transverse lung-window CT (1.0-mm thickness) scans obtained at levels of suprahepatic inferior vena cava (**a**) and liver dome (**b**), respectively, show bronchial wall thickening, tree-in-bud opacities (*arrows*) and small nodules (arrowheads) in both lungs. **c** Medium-magnification photomicrograph shows bronchiolar wall thickening (*arrows*) due to dense inflammatory cells infiltration (eosinophils and lymphocytes) and lymphoid follicle (*arrowheads*) formation. Also note pneumonic area (*asterisk*) in alveolar spaces. (Hematoxylin-eosin stain, original magnification ×40) **d** High-magnification photomicrograph demonstrates necrotizing vasculitis (*arrows*) involving alveolar wall capillary. Capillary wall is thickened with eosinophil infiltration and necrosis. (Hematoxylin-eosin stain, original magnification ×400)

34±24.1 days) of 11 with a CT airway disease pattern and seven of eight with an airspace disease pattern (within 23–140 days of follow-up, mean 70±44.3 days) showed complete radiologic abnormality resolution at follow-up. At the time of writing, one patient had died (1 year after diagnosis) due to congestive heart failure, and the remaining 18 patients had survived with or without disease relapse. Seven patients suffered from repeated relapse and remission (Table 2). Four of these seven patients underwent follow-up CT examinations. When relapse occurred, the relapsing pattern was identical to the initial presentation in one patient (the initial airspace pattern) and different in the remaining three patients (they had the initial airway pattern, but showed airspace pattern at recurrence).

Discussion

The pathologic findings of CSS show asthmatic bronchitis, eosinophilic pneumonia, extravascular stellate granulomas, and vasculitis [1, 14]. In a comparative study of TSCT findings and histopathologic study of lung biopsy specimens, Choi et al. [5] reported that consolidation corresponded histologically to areas of eosinophilic pneumonia,

Table 3 Distribution of lung parenchymal abnormalities at thin-section CT in 19 patients with CSS (*GGO* ground-glass opacity)

	Small nodules (*n*=12, 63%)	GGO (*n*=10, 53%)	Consolidation (*n*=8, 42%)	Tree-in-bud signs (*n*=7, 37%)	Interlobular septal thickening (*n*=8, 42%)
Transverse plane					
Peripheral	4	4	2	2	7
Central	0	0	0	0	0
Random	8	6	6	5	1
Longitudinal plane					
Upper	0	3	0	0	0
Lower	2	3	4	0	3
Random	10	4	4	7	5
Peribronchovascular	0	1	3	3	1

whereas bronchial wall thickening corresponded to areas of asthmatic bronchitis. Moreover, multiple variable-sized nodules corresponded to areas of necrotizing granulomatous vasculitis with eosinophilic infiltration. More recently, Silva et al. [15] suggested that interlobular septal thickening may be histopathologically due to septal edema, eosinophilic infiltration, and mild fibrosis. In addition to the previously reported results [5, 15], in the present study, small centrilobular nodules at TSCT corresponded to the areas of bronchiolar wall thickening (with eosinophilic and lymphocytic infiltration) and surrounding necrotizing capillaritis in alveolar walls. Nodules (>10 mm in diameter) at TSCT corresponded histopathologically to mixed areas of pulmonary hemorrhage related to capillaritis, necrotizing granulomas, and surrounding eosinophilic infiltration.

In our study, reversed halo sign was observed in one patient with CSS. Thus, when reversed halo sign is identified at TSCT, differential diagnoses should include cryptogenic organizing pneumonia, chronic eosinophilic pneumonia, fungal infection such as paracoccidioidomycosis, and finally CSS [8, 16, 17].

In our study, CT findings were classifiable into airway or airspace disease patterns. Airway patterns consisted mainly of small centrilobular nodules and tree-in-bud sign, bronchial dilatation and wall thickening, and mosaic perfusion pattern, whereas airspace patterns consisted of GGO, consolidation, and poorly-defined nodules. Moreover, this classification seems to help predict radiologic response of lung abnormalities to treatment, i.e., patients with an airspace pattern at CT responded more readily to treatment than those with an airway pattern.

Because asthma is present in almost all CSS patients and because it causes bronchial or bronchiolar wall thickening and small centrilobular nodules and tree-in-bud sign at TSCT [2, 18, 19], one might conclude that airway abnormality pattern in CSS is simply due to airway involvement in asthma. However, in patients with a CT airway pattern, some areas of GGO were also observed in addition to bronchial or bronchiolar wall thickening and small centrilobular nodules and tree-in-bud sign. Moreover, pathologic specimens obtained from small nodular areas demonstrated necrotizing capillaritis in peribronchiolar interstitium and eosinophilic bronchiolitis. Therefore, the CT airway disease pattern appears to result from combination of eosinophilic bronchitis, bronchiolitis and alveolitis, and surrounding alveolar wall necrotizing vasculitis.

Clinically, CSS shows three distinct phases: (1) a prodromal phase that may persist for many years, consisting of asthma and often preceding allergic rhinitis; (2) a phase of marked peripheral blood eosinophilia and eosinophilic tissue infiltrates resembling Löffler's syndrome, or chronic eosinophilic pneumonia, which may recur over a period of years; (3) a life-threatening vasculitic phase [20]. However, it appears that these three phases do not always manifest in this order. In our patients, the initial CT patterns of parenchymal lesions were divisible into airway and airspace patterns. In addition, patients with an airspace pattern (the eosinophilic pneumonic or vasculitic phase) responded more readily to therapy than those with an airway pattern (probably the prodromal phase). Moreover, asthma treatment durations were not different for airway and airspace disease patterns.

Our study is limited by its retrospective nature. In addition, CT-pathologic and CT-PFT comparisons were not performed in all patients. Moreover, follow-up evaluation studies were performed mainly using chest radiography, and only seven patients underwent follow-up CT. Therefore, detailed treatment-associated changes, such as small centrilobular nodules, tree-in-bud sign, and mosaic perfusion pattern, may not have been identified.

In conclusion, about three-quarters of patients with CSS show parenchymal lung lesions at CT. These consist predominantly of small centrilobular nodules and tree-in-bud sign, GGO, consolidation, bronchial dilatation or wall thickening, interlobular septal thickening, and mosaic perfusion pattern. The study shows that lung lesion CT findings in CSS allow their classification into airway or airspace disease pattern, and this classification seems to be related to PFT results, underlying histopathologies, and treatment response.

References

1. Churg J, Strauss L (1951) Allergic granulomatosis, allergic angiitis, and periarteritis nodosa. Am J Pathol 27:277–301
2. Lanham JG, Elkon KB, Pusey CD, Hughes GR (1984) Systemic vasculitis with asthma and eosinophilia: a clinical approach to the Churg-Strauss syndrome. Medicine 63:65–81
3. Masi AT, Hunder GG, Lie JT, Michel BA, Bloch DA, Arend WP, Calabrese LH, Edworthy SM, Fauci AS, Leavitt RY et al (1990) The American College of Rheumatology 1990 criteria for the classification of Churg-Strauss syndrome (allergic granulomatosis and angiitis). Arthritis Rheum 33:1094–1100
4. Chumbley LC, Harrison EG Jr, DeRemee RA (1977) Allergic granulomatosis and angiitis (Churg-Strauss syndrome). Report and analysis of 30 cases. Mayo Clin Proc 52:477–484
5. Choi YH, Im JG, Han BK, Kim JH, Lee KY, Myoung NH (2000) Thoracic manifestation of Churg-Strauss syndrome: radiologic and clinical findings. Chest 117:117–124
6. Worthy SA, Muller NL, Hansell DM, Flower CD (1998) Churg-Strauss syndrome: the spectrum of pulmonary CT findings in 17 patients. AJR Am J Roentgenol 170:297–300

7. Mountain CF, Dresler CM (1997) Regional lymph node classification for lung cancer staging. Chest 111:1718–1723
8. Kim SJ, Lee KS, Ryu YH, Yoon YC, Choe KO, Kim TS, Sung KJ (2003) Reversed halo sign on high-resolution CT of cryptogenic organizing pneumonia: diagnostic implications. AJR Am J Roentgenol 180:1251–1254
9. Tuddenham WJ (1984) Glossary of terms for thoracic radiology: recommendations of the Nomenclature Committee of the Fleischner Society. AJR Am J Roentgenol 143:509–517
10. Austin JH, Muller NL, Friedman PJ, Hansell DM, Naidich DP, Remy-Jardin M, Webb WR, Zerhouni EA (1996) Glossary of terms for CT of the lungs: recommendations of the Nomenclature Committee of the Fleischner Society. Radiology 200:327–331
11. Lee KS, Kim TS, Han J, Hwang JH, Yoon JH, Kim Y, Yoo SY (1999) Diffuse micronodular lung disease: HRCT and pathologic findings. J Comput Assit Tomogr 23:99–106
12. Quanjer PH, Tammeling GJ, Cotes JE, Pedersen OF, Peslin R, Yernault JC (1993) Lung volumes and forced ventilatory flows. Report working party standardization of lung function tests, European community for steel and coal. Official statement of the European respiratory society. Eur Respir J Suppl 16:5–40
13. Silva CI, Colby TV, Muller NL (2004) Asthma and associated conditions: high-resolution CT and pathologic findings. AJR Am J Roentgenol 183:817–824
14. Lanham J, Churg J (1991) Churg-Strauss syndrome. In: Churg A, Churg J (eds) Systemic vasculitides. Igaku-Shoin, New York, pp 110–120
15. Silva CI, Muller NL, Fujimoto K, Johkoh T, Ajzen SA, Churg A (2005) Churg-Strauss syndrome: high resolution CT and pathologic findings. J Thorac Imaging 20:74–80
16. Voloudaki AE, Bouros DE, Froudarakis ME, Datseris GE, Apostolaki EG, Gourtsoyiannis NC (1996) Crescentic and ring-shaped opacities. CT features in two cases of bronchiolitis obliterans organizing pneumonia (BOOP). Acta Radiol 37:889–892
17. Gasparetto EL, Escuissato DL, Davaus T, de Cerqueira EM, Souza AS Jr, Marchiori E, Muller NL (2005) Reversed halo sign in pulmonary paracoccidioidomycosis. AJR Am J Roentgenol 184:1932–1934
18. Lynch DA, Newell JD, Tschomper BA, Cink TM, Newman LS, Bethel R (1993) Uncomplicated asthma in adults: comparison of CT appearance of the lungs in asthmatic and healthy subjects. Radiology 188:829–833
19. Grenier P, Mourey-Gerosa I, Benali K, Brauner MW, Leung AN, Lenoir S, Cordeau MP, Mazoyer B (1996) Abnormalities of the airways and lung parenchyma in asthmatics: CT observations in 50 patients and inter-and intraobserver variability. Eur Radiol 6:199–206
20. Cottin V, Cordier JF (1999) Churg-Strauss syndrome. Allergy 54:535–551